Electronic Supplementary Information.

Spontaneous aggregation of lithium ion coordination polymers in fluorinated electrolytes for high-voltage batteries.

Christos D. Malliakas, Kevin Leung, Krzysztof Z. Pupek, Ilya A. Shkrob, and Daniel P. Abraham

Full acknowledgments

This work was supported by the US-DOE Office of Science, Division of Chemical Sciences, Geosciences and Biosciences under contracts No. DE-AC02-06CH11357 to Argonne. The submitted manuscript has been created by UChicago Argonne, LLC, Operator of Argonne National Laboratory ("Argonne"). Argonne, a U.S. Department of Energy Office of Science laboratory, is operated under Contract DE-AC02-06CH11357.

K. L. was supported by Nanostructures for Electrical Energy Storage (NEES), an Energy Frontier Research Center funded by the U.S. Department of Energy, Office of Science, Office of Basic Energy Sciences under Award No. DESC0001160. Sandia National Laboratories is a multiprogram laboratory managed and operated by Sandia Corporation, a wholly owned subsidiary of Lockheed Martin Corporation, for the U.S. Department of Energy's National Nuclear Security Administration under contract DE-AC04-94AL85000.

C. D. M. was supported by the U.S. Department of Energy, Office of Science, Materials Sciences and Engineering Division. Use was made of the IMSERC X-ray Facility at Northwestern University.

S1. Experimental and computational detail.

Materials. Battery grade fluoroethylene carbonate was obtained from Solvay. Battery grade bis(2,2,2-trifluoroethyl)carbonate was produced at Argonne's Materials Engineering Research Facility (MERF) facility.

Lithium hexafluorophosphate was obtained from Strem Chemicals, and all other materials were obtained from Sigma Aldrich. All solutions and operations were handled in inert atmosphere inside an argon filled glove box containing ppm level of oxygen and water at 25 ^{o}C. The solutions were prepared by stirring the weighed amounts of material for 1-2 hours; in some cases warming of the sample to 40-50 ^{o}C and periodic vortexing was used to accelerate dissolution. The prepared solutions were stored in glove boxes with minimal exposure to light (the containers were wrapped in aluminum foil) and minimal disturbance. Once crystallization started, the crystals formed rapidly (probably, in less than 2-3 hours). ^{19}F NMR showed no evidence for the presence of impurities or (photo)degradation of these materials. Spontaneous crystallization from FEC:BFEC solutions was observed on two separate occasions in two laboratories and involved 20-50 mL solutions prepared from different batches of these solvents. One one occasion it occurred after 2 months of storage in a fluoropolymer (PFA) container. One another occasion it occurred after only 2 weeks of storage in a glass container.

To separate solid precipitate, the solutions (after Ostwald ripening that took several days) were centrifuged at 3000 rpm in sealed 1.5 mL plastic tubes, the supernate was removed and anhydrous toluene added, and the residue was resuspended by vortexing). This operation was repeated 10X to remove all traces of the solvent that is not part of the solvate crystals. The remaining material was either dried in a flow of inert gas (for XRD analysis) or dissolved in dimethylsulfoxide-d_6 for NMR analysis. Ripening and complete phase separation were especially rapid and efficient in 1.35 M solutions, but they were also sometimes observed at lower concentration of $LiPF_6$ (above 0.8 M) albeit taking even longer time. In 1.35 M solutions, the phase separation was reproducible and occurred in less than a week.

X-ray crystallography. Single-crystal X-ray diffraction data on a crystal of $Li(FEC)_3PF_6$ were collected with the use of monochromatized (QuazarTM-optics) Mo Kα radiation (λ = 0.71073 Å) on a Bruker Kappa APEXII CCD diffractometer. The crystal was removed from the mother liquor (4:1 w/w BFEC:FEC containing 1 M $LiPF_6$) with a cryoloop and frozen to 100 K. The crystal-to-detector distance was 4 cm. Data were collected at different ω and φ scans at a step of 0.5º with an exposure time of 4 s/frame. The collection of the intensity data was carried out with the program *SMART*. [1] Cell refinement and data reduction were carried out with the use of the program *SAINT*, [1] and a face-indexed absorption correction was performed numerically with the use of the program *XPREP*. [2, 3] Then the program *SADABS* [4] was used to make incident beam and decay corrections. The structures were solved with the direct-methods program *SHELXS* [3] and refined with the least-squares program *SHELXL*. [2] The resulting structure is loaded to Cambridge Crystallographic Data Center (CCDC) base, entry 1452270.

Powder X-ray diffractometry. The powder diffractograms were obtained at ambient temperature using a Bruker D8 Advance diffractometer (Cu Kα radiation of 40 mA, 40 kV, λ = 0.15418 nm). The data were analyzed using DIFFRAC.SUITE EVA software (Bruker). The powder sample was placed inside an airtight plastic dome specimen holder (Bruker A100B36) mounted on a homemade assembly allowing purging of dry Ar through the assembly during the signal acquisition. The diffraction pattern stayed constant over two hours required to obtain good quality data despite the extreme moisture sensitivity of the sample. This constancy was ensured by collecting the data in series of 15 min exposure and then inspection of the data for systematic changes. The computed powder spectrum in **Figure S2** was calculated from the single crystal data (obtained at 100 K) using Mercury (Version 3.6, CCDC) software. We remind the reader that the powder diffraction data were obtained at room temperature, while the single crystal data were obtained at low temperature, so some small differences between lattice parameters and positions of the Bragg peaks are entirely expected. The broad feature in the diffractogram originates from an amorphous component in the powder.

^{7}Li and ^{19}F NMR (Nuclear Magnetic Resonance) spectroscopy. ^{7}Li and ^{19}F NMR spectra were obtained using a Bruker Avance III HD 300 MHz spectrometer. 10 vol% CDCl3 was added for frequency locking. 10 s acquisition time and 15 s interval between the 90^o excitation pulses were used to avoid saturation of the NMR transitions. 200-500 pulses were used to obtain the sufficient quality for accurate numerical integration. The ^{19}F shifts (in parts per million, ppm) are given vs. $CFCl_3$ and ^{7}Li shifts are given vs. 1 M LiCl in D_2O. We remind the reader that slow rotation of molecular aggregates in solution precludes their direct observation by solution Fourier transform NMR, as the resonance lines become extremely broadened (so the corresponding free induction decay occurs within the dead time of the spectrometer). For this reason, even in

solutions where the aggregates were present, only smaller (rapidly rotating, slowly relaxing) Li^+ ion clusters are observed. We also remind that ^7Li nucleus is quadrupolar (I=3/2) and the NMR line width is largely determined by sphericity of the crystal field around a Li^+ ion. The transition from the tetrahedral to octahedral coordination would be observed not only in the chemical shift, but also through the line shape; neither were observed either below or above the critical point (for free Li^+ ions remaining in the solution). Our conclusion is that the nature of the solvation complexes (for free Li^+ ions) does not change as a function of concentration and it is the same for FEC and EC. Once the aggregation occurs, the aggregates become so large that their rotation is slow, the relaxation is rapid, and such species are not observed by solution NMR at all. There seems to be no intermediate concentration ranges, in which smaller aggregates (the "seeds" of crystallization) coexist with the free Li^+ ion complexes. Once the "seed" is formed, it rapidly grows to mesoscale size.

Semiempirical calculations. PM7 method [5, 6] from MOPAC2012 suite [7, 8] was used in all of the semiempirical calculations. (L)BFGS algorithm was used for geometry optimization. PM7 is the latest implementation of the MNDO/NNDO family of semiempirical methods that are specially designed for solid and crystalline materials and tested extensively on molecular and ionic crystals. [5, 6] The motivation for using such methods is that DFT method is not significantly better in estimating energetics for such crystals than semiempirical methods, while being more time consuming. Since the structure is already known, the question is only how much refinement one can expect from a given method and what insights one can obtain from such calculations.

The starting configurations for gas phase clusters were selected from AMBER field optimized clusters. Both symmetrized and asymmetric configurations were considered at PM7 level, and some of the asymmetric ones were then additionally symmetrized. On average 3-4 starting configurations were considered, but for some clusters more were explored due to the shallow potential surface minima. For crystal phase calculations the initial configuration was the crystal structure of the material as determined in our experiments.

DFT calculations. Gas phase density functional theory (DFT) calculations with geometry optimization were performed using B3LYP functional [9, 10] and 6-31+G(d,p) basis set from Gaussian 03 suite. [11] The input geometries in these calculations were preoptimized using MNDO method from the same suite.

AIMD calculations. In this method, all species are treated at DFT level, and periodic boundary conditions are applied to a cubic cell. After pre-equilibration using classical force field-based molecular dynamics, AIMD simulations were carried out at finite temperature via solving Newton's equation of motion. [12, 13] The VASP code [14-16] and the PBE functional [17] were applied in these simulations. G-point Brillouin zone sampling and a 400 eV plane wave energy cut off were enforced. Tritium masses were substituted for protons, which enabled the use of 1.0 fs time steps without affecting structural properties, although dynamical properties predicted (not shown) would not necessarily correspond to realistic conditions. Five separate calculations were carried out, using Nosé thermostats to control the average temperature at T=300 K or T=400 K. The binning of Li-X g(r) histograms was 0.05 Å, and the cutoff radius for coordination number (CN) calculations was 2.7 Å. This cutoff distance roughly corresponds to the first minimum in the g(r) plots shown in Figure 3. Five models were examined:

(i) & (ii): 2 $LiPF_6$ and 30 FEC molecules placed inside a 15.7 Å x 15.7 Å x 15.7 Å cell box (corresponding to the mass density of 1.496 g/cm^3 and molar concentration of 0.86 M $LiPF_6$). The trajectories were run for (i) 23.7 ps at T=300 K and (ii) 20.0 ps at T=400 K, respectively. The higher temperature simulation should yield better statistical sampling. Nevertheless, these trajectories yield almost identical average coordination numbers (CNs) between Li^+ ion and atoms in the electrolyte molecules: 3.0 for carbonyl oxygen (O_{CO}), 0.0 for FEC ring oxygen (O_r), 0.0 for fluorine atom in FEC, and 1.2 for fluorine atom in PF_6^- anion. Since the results are not strongly dependent on temperature, in Figure 3 we have only presented the results obtained at 300 K.

(iii) & (iv): One Li^+ ion and 32 FEC molecules placed inside a 15.7x15.7x15.7 A^3 box. The durations of trajectories kept at (iii) T=300 K and (iv) T=400 K are 16.5 and 13.8 ps, respectively. Here the results are slightly more temperature dependent. The coordination numbers between Li^+ and O_{CO}, O_r, and F are 3.9, 0.0, and 0.0 at T=300 K, and are 3.6, 0.0, and 0.2 at T=400 K. Nevertheless, both sets of computations indicate that Li^+ predominately coordinates to O_{CO}, with only minor coordination to F, even in the absence of PF_6^- anions.

(v) isolated $Li(FEC)_6^+$ cluster placed inside a 16 Å x 16 Å x 16 Å box. The trajectories were ran for 9 ps at 300 K. The initial configurations were PM7 optimized structures (for n=6 in Table 4S). Regardless of the initial orientation of FEC molecules (with oxygens or fluorines in the first coordination sphere), the equilibrated structures always had only oxygen atoms in this sphere with CN of four and 3-4 carbonyl oxygens at Li-O less than 2.2 Å. The charge was compensated by a uniformly charged background. This is a standard practice in AIMD and classical MD simulations. See [18] and references therein. In particular, refs. 8-9 therein [19, 20] have shown that the solvation free energy of an ion in a high-dielectric liquid and uniformly compensating background converge rapidly with simulation cell size. The FEC liquid should have a sufficiently large dielectric constant to make this correct in this case as well.

Table S1.

Chemical shifts (δ) and Gaussian widths (σ) for nuclear magnetic resonance lines from ^{7}Li nuclei in solvated Li^{+} ions for selected $LiPF_6$ solutions in (fluoro)organic carbonates. [a]

[LiPF], M	solvent	δ (^{7}Li) ppm [b]	σ, Hz
0.35	PC	-0.88	6.1
0.12	FEC	-0.60	5.9
0.85	FEC	-0.56	6.8

a) contained 10 wt% $CDCl_3$ for frequency locking;

b) parts per million with respect to 1 M LiCl in D_2O;

Table S2.

Comparison of experimentally determined and calculated [a] unit cell parameters and energetics for *Z*=2 crystal polymorphs of $[LiL_6]PF_6$.

	L	***a*, Å**	***b*, Å**	***c*, Å**	**α, °**	**β, °**	**γ, °**	**volume, Å^3**	**Space group**	**Heat of formation, kcal/mol.eq**
Exp.	FEC	5.513	13.009	13.009	120	90	90	808.0	P -3	-
Calc.	FEC	6.123	13.418	14.404	123.43	90 [b]	90 [b]	987.6	P 1 2 1	-1058.97060
Calc.	FEC	5.238	13.828	14.262	121.017	87.51	102.38	850.0	P 1	-1066.45981
Calc.	EC	4.613	14.067	14.191	120.91	91.62	89.00	789.81	P 1	-926.690005
Calc.	PC	6.096	13.79	14.263	118.42	91.34	86.49	1052.54	P 1	-944.398755
Calc.	DMC	6.022	13.894	13.991	120.48	95.68	103.58	946.75	P 1	-922.35594

a) PM7 semiempirical method from MOPAC2012 suite. Note that in this table the cell axes for $[Li(FEC)_3]PF6$ crystal are listed in a different order than in the text to facilitate the comparison with calculated triclinic cells.

b) fixed angles

Table S3.

Comparison of experimentally determined and calculated bond and charge parameters for *Z*=2 crystal polymorphs of $[LiL_6]PF_6$.

	L	*Li ion* [b]	*C=O* [b]	*Li-O*, Å [a]	*Li-Li*, Å
Exp.	**FEC**	**-**	**-**	**2.09**	**2.76**
Calc.	FEC	0.844	-0.582	2.16	2.62
Calc.	EC	0.823	-0.611	2.19	2.28
Calc.	PC	0.863	-0.569	2.22	3.04
Calc.	DMC	0.865	-0.615	2.31	3.02

B3LYP/6-31+G(d,p) model.

a) mean distance to the closest atoms

b) atomic charges by Mulliken population analysis

Table S4.

Comparison of calculated bond lengths and energetics for LiL_n^+ species in the gas phase (PM7 method from MOPAC2012 suite)

nearest atoms to Li^+ ion [a]	*n*	*sym. point grp.*	*bond lengths, Å*	*Heat of formation, kcal/mol*	*bonding energy per ligand, eV*	E_{rel}, [b] eV
L=FEC						
$4O_{CO}$	4	C_2	2.12	-610.937	-1.03	2.00
$5O_{CO}$	5	C_1	2.17	-787.326	-0.91	1.57
$4O_{CO}$, O_r	5	C_1		-795.562	-0.98	1.21
3CO+2O	5	C_1		-800.276	-1.02	1.01
$3O_{CO}$, $3O_r$	6	C_3		-968.362	-0.86	0.93
$6O_{CO}$	6	S_6	2.26	-970.106	-0.88	0.85
$5O_{CO}$, O_r	6	C_1		-978.415	-0.94	0.49
$2O_{CO}$, $2O_r$, 2F	6	C_2		-981.141	-0.96	0.38
$3O_{CO}$, 3F	6	C_3	2.20, 2.11	-983.556	-0.97	0.27
$2O_{CO}$, $2O_r$, 2F	6	C_i	2.08, 2.45, 1.92	-987.649	-1.00	0.09
$2O_{CO}$, 4F	6	C_i	2.09, 1.96	-989.791	-1.02	0.00
L=EC						
$4O_{CO}$	4	C_2	2.10	-418.02	-1.03	1.28
$5O_{CO}$	5	C_1		-549.05	-0.94	0.73
$4O_{CO}$, O_R	5	C_1	2.19	-551.478	-0.96	0.62
$6O_{CO}$	6	S_6	2.27	-680.771	-0.88	0.15
$4O_{CO}$, $2O_R$	6	C_2	2.19, 2.34	-683.126	-0.90	0.05
$3O_{CO}$, $3O_R$	6	C_3	2.10, 2.44	-684.216	-0.91	0.00

a) see **Figure S5**; O_{CO} is the carbonyl oxygen and O_r is the ring oxygen

b) energy of $LiL_n^+ + (6-n)L$ vs. the lowest energy cluster.

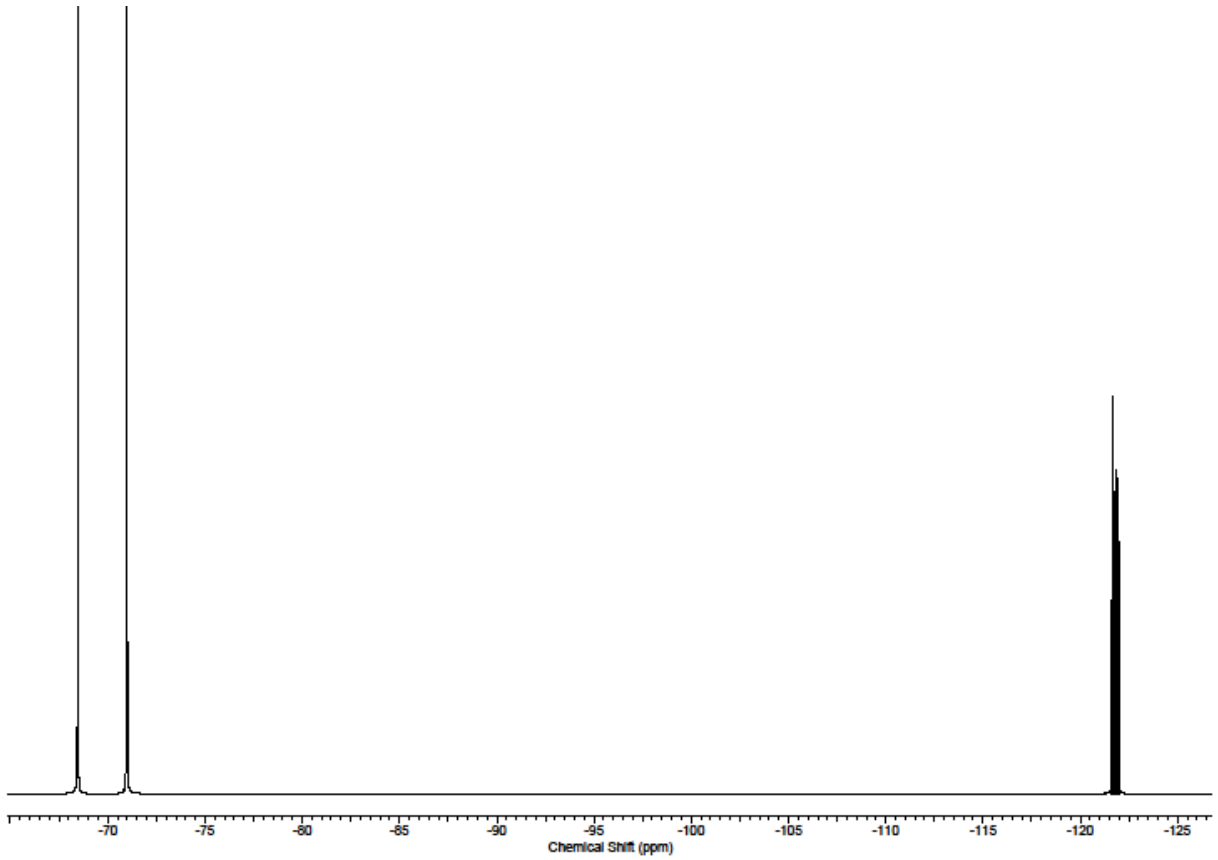

Figure S1. The 300 MHz ^{19}F NMR spectrum of dilute dimethylsulfoxide-d_6 solution containing the dissolved crystalline precipitate that was multiply washed with anhydrous toluene. The chemical shift in parts per million is given vs. $CFCl_3$. The doublet at -73.1 ppm is from the hexafluorophosphates anions ($^3J(^{19}F\text{-}^{31}P)$ = 711 Hz), while the two overlapping multiplets of resonance lines with the chemical shifts between -122 and -122.5 ppm are from the fluorine-19 in FEC. BFEC (which is not observed) would appear as a triplet at -72.9 ppm ($^3J(^{19}F\text{-}^{1}H)$ = 8.2 Hz). From integration of the resonance lines, 1:3 mol/mol stoichiometry ($LiPF_6$: FEC) was established.

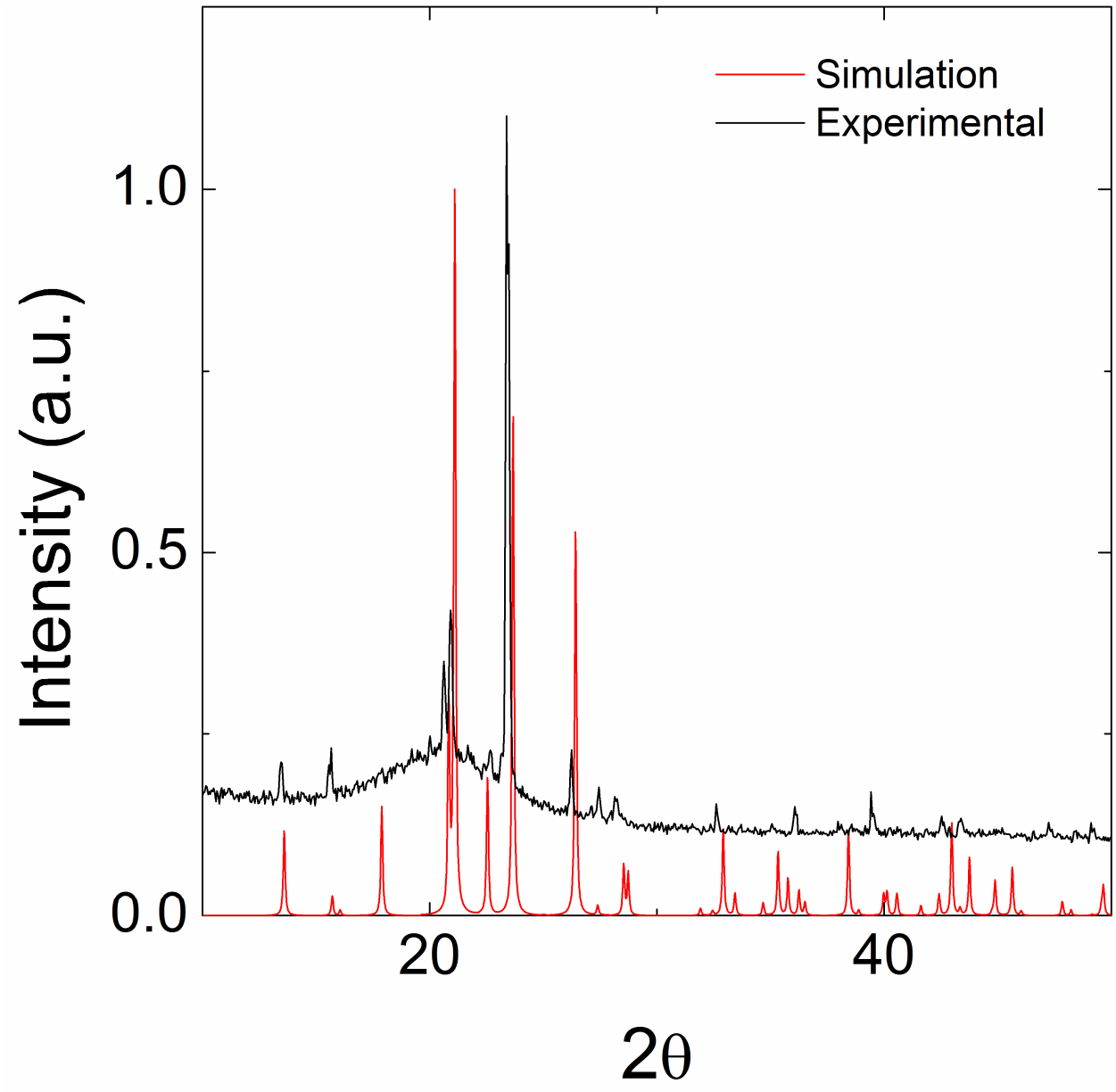

Figure S2. Comparison between the experimental powder X-ray diffraction pattern (black line) for $[Li(FEC)_3]PF_6$ with the simulated pattern using the single crystal data (red line). Here θ is the scattering angle.

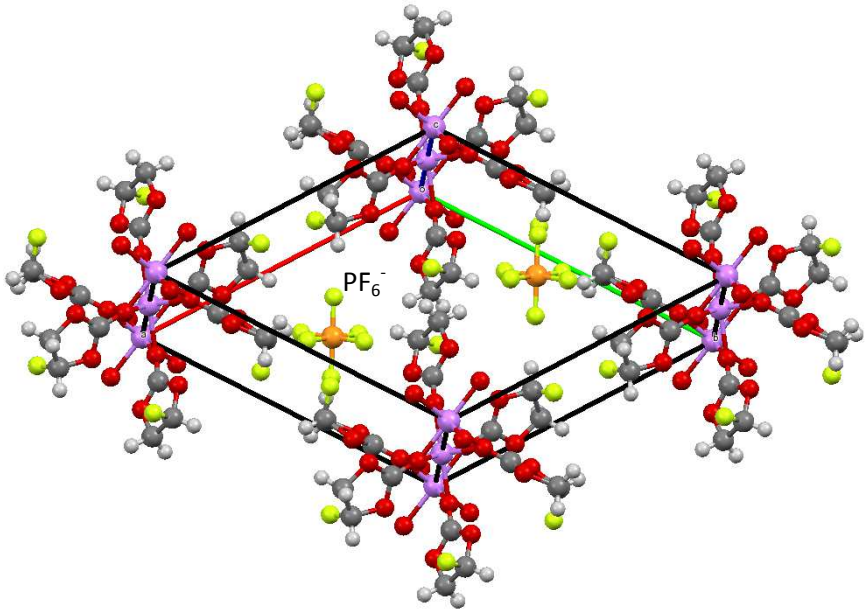

Figure S3. The unit cell of $[Li(FEC)_3]PF_6$ crystal (Z=2 experimental structure). Li^+ cations form the infinite chains along crystallographic axis c in which each Li^+ ion is octahedrally coordinated by six carbonyl oxygens in FEC molecules and each carbonyl oxygen of FEC is shared by two Li^+ ions. Purple atoms are lithium, green atoms are fluorine, dark grey atoms are carbon, red atoms are oxygen, and and light grey atoms are hydrogen.

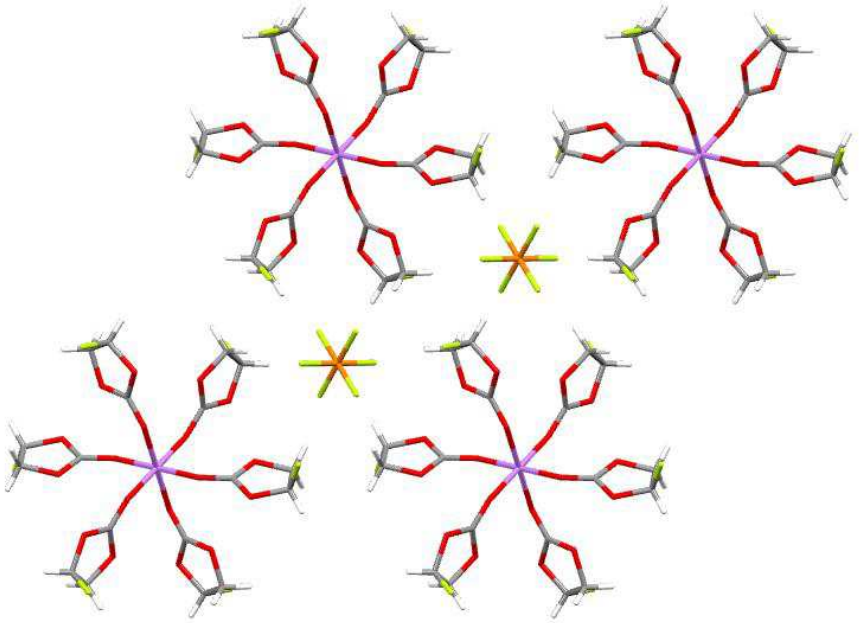

Figure S4. The view of $[Li(FEC)_3]PF_6$ crystal lattice with crystallographic axis ***c*** perpendicular to the plane of the figure.

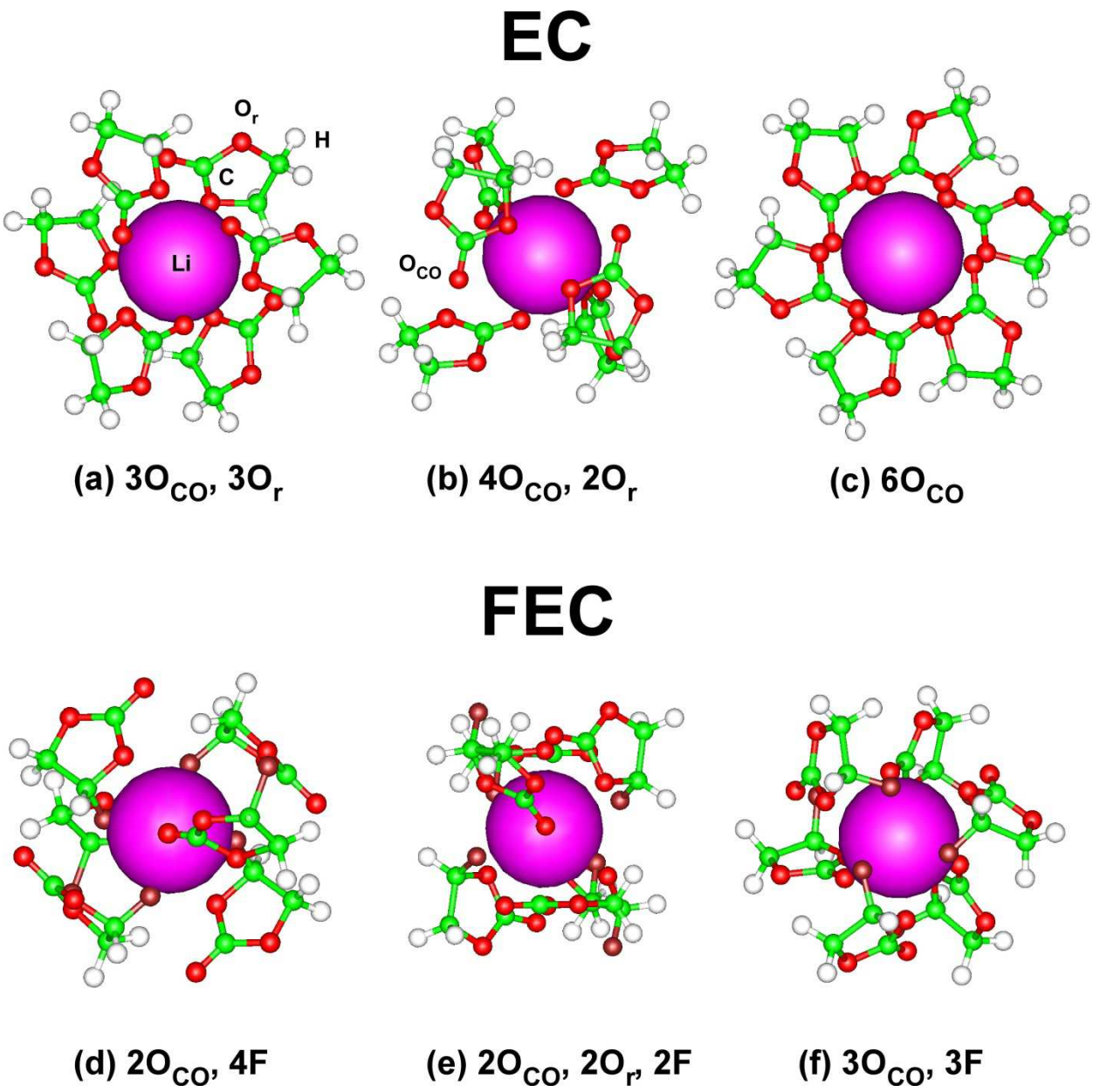

Figure S5. Structural representations for the lowest energy, optimized geometry LiL_6^+ clusters in the gas phase (PM7 method from MOPAC2012 suite) for (a-c) L=EC and (d-f) L=FEC. The legends list the atoms in the first coordination spheres of these cluster ions. See Table S4 for energetics and bond lengths.

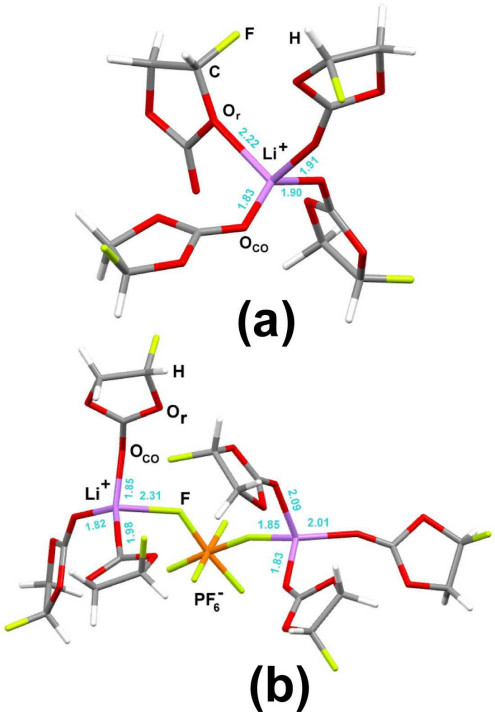

Figure S6. Snapshots of the typical Li^+ ion solvated structures found in systems (a) and (b), respectively. The Li-X distances are indicated in the plot.

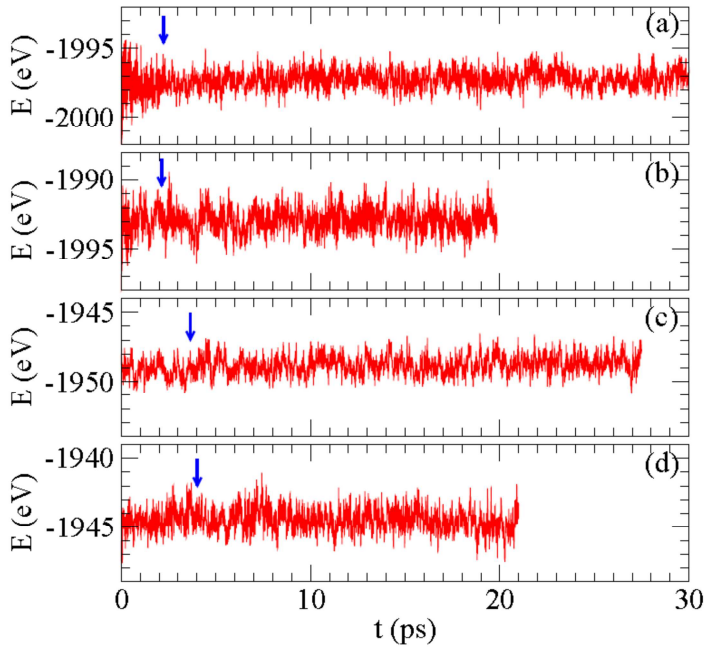

Figure S7. Potential energies as functions of time for AIMD computations involving 32 FEC molecules and (a) Li^+ ion at *T*=300 K and (b) *T*=400 K; (c) two Li^+ ions and two PF_6^- anions at *T*=300 K and (d) *T*=400 K. The blue arrow indicate the beginning of the trajectory after pre-equilibration.

Additional references.

(1) Bruker *Smart Version 5.054 Data Collection and Saint-Plus Version 6.45a Data Processing Software for the Smart System* Bruker AXS Instruments, Inc. : Madison, WI, USA, 2003.

(2) Sheldrick, G. M. *Shelxtl*, 6.14; Bruker AXS Instruments, Inc.: Madison, Wisconsin, USA, 2003.

(3) Sheldrick, G. M. A Short History of Shelx. *Acta Crystallogr. A* **2008,** *64*, 112-122.

(4) Sheldrick, G. M. *Sadabs: Bruker/Siemens Area Detector Absorption and Other Corrections*, 2.03; Bruker AXS Inc.: Madison, Wisconsin, USA., 2008.

(5) Hostaša, J.; Řezáča, J.; Hobzaa, P. On the Performance of the Semiempirical Quantum Mechanical PM6 and PM7 Methods for Noncovalent Interactions. *Chem. Phys. Lett.* **2013,** *568-569*, 161-166.

(6) Stewart, J. P. Optimization of Parameters for Semiempirical Methods VI: More Modifications to the NDDO Approximations and Re-Optimization of Parameters. *J. Mol. Model.* **2013,** *19*, 1-32.

(7) Stewart, J. J. P. Mopac2012.

(8) Maia, J. D. C.; Carvalho, G. A. U.; Mangueira, C. P.; Santana, S. R.; Cabral, L. A. F.; Rocha, G. B. GPU Linear Algebra Libraries and GPGPU Programming for Accelerating MOPAC Semiempirical Quantum Chemistry Calculations. *J. Chem. Theory Comput.* **2012,** *8*, 3072-3081.

(9) Becke, A. D. Density-Functional Exchange-Energy Approximation with Correct Asymptotic Behavior. *Phys. Rev. A* **1988,** *38*, 3098-3100.

(10) Lee, C.; Yang, W.; Parr, R. G. Development of the Colle-Salvetti Correlation-Energy Formula into a Functional of the Electron Density. *Phys. Rev. B* **1988,** *37*, 785-789.

(11) Frisch, M. J.; Trucks, G. W.; Schlegel, H. B.; Scuseria, G. E.; Robb, M. A.; Cheeseman, V. G.; Montgomery, J. A., Jr.; Vreven, K. N.; Kudin, J. C.; Burant, J. C. *Gaussian 03, Rev. C.02*, Gaussian, Inc.: Wallingford CT, 2004.

(12) Car, R.; Parrinello, M. Unified Approach for Molecular Dynamics and Density-Functional Theory. *Phys. Rev. Lett.* **1985,** *55*, 2471-2474.

(13) Kuhne, T. D. Second Generation Car–Parrinello Molecular Dynamics. *WIREs Comp. Mol. Sci.* **2014,** *4*, 391–406.

(14) Kresse, G.; Joubert, D. From Ultrasoft Pseudopotentials to the Projector Augmented-Wave Method. *Phys. Rev. B* **1999,** *59*, 1758-1775.

(15) Kresse, G.; Furthmuller, J. Efficiency of Ab-Initio Total Energy Calculations for Metals and Semiconductors Using a Plane-Wave Basis Set. *Comp. Mater. Sci.* **1996,** *6*, 15-50.

(16) Kresse, G.; Furthmuller, J. Efficient Iterative Schemes for *Ab Initio* Total-Energy Calculations Using a Plane-Wave Basis Set. *Phys. Rev. B* **1996,** *54*, 11169-11186.

(17) Perdew, J. P.; Burke, K.; Ernzerhof, M. Generalized Gradient Approximation Made Simple. *Phys. Rev. Lett.* **1996,** *77*, 3865-3868.

(18) Leung, K.; Rempe, S. B.; von Lilienfeld, O. A. *Ab Initio* Molecular Dynamics Calculations of Ion Hydration Free Energies. *J. Chem. Phys.* **2009,** *130*, 204507 (11 pages).

(19) Hummer, G.; Pratt, L. R.; García, A. E. Ion Sizes and Finite-Size Corrections for Ionic-Solvation Free Energies. *J. Chem. Phys.* **1997,** *107*, 9275-9277.

(20) Hummer, G.; Pratt, L. R.; García, A. E. Free Energy of Ionic Hydration. *J. Phys. Chem.* **1996,** *100*, 1206–1215.